Biometrics via Oculomotor Plant Characteristics: Impact of Parameters in Oculomotor Plant Model

OLEG KOMOGORTSEV, COREY HOLLAND, ALEX KARPOV, AND LARRY R. PRICE Texas State University

This paper proposes and evaluates a novel biometric approach utilizing the internal, non-visible, anatomical structure of the human eye. The proposed method estimates the anatomical properties of the human oculomotor plant from the measurable properties of human eye movements, utilizing a two-dimensional linear homeomorphic model of the oculomotor plant. The derived properties are evaluated within a biometric framework to determine their efficacy in both verification and identification scenarios. The results suggest that the physical properties derived from the oculomotor plant model are capable of achieving 20.3% equal error rate and 65.7% rank-1 identification rate on high-resolution equipment involving 32 subjects, with biometric samples taken over four recording sessions; or 22.2% equal error rate and 12.6% rank-1 identification rate on low-resolution equipment involving 172 subjects, with biometric samples taken over two recording sessions.

Categories and Subject Descriptors: **I.2.10 [Artificial Intelligence]**: Vision and Scene Understanding—*Modeling and recovery of physical attributes*; **I.5.1 [Pattern Recognition]**: Models—*Structural*; **I.6.4 [Simulation and Modeling]**: Model Validation and Analysis

General Terms: Biometrics

Additional Key Words and Phrases: Human oculomotor system, biological system modeling, mathematical model, security and protection.

ACM Reference Format:

Komogortsev, O., Holland, C., Karpov, A., and Price, L. R. 2014. Oculomotor Plant Characteristics: Biometric Performance Evaluation. *ACM Trans. Appl. Percept.* 2, 3, Article 1 (May 2014), 13 pages.

DOI:http://dx.doi.org/10.1145/0000000.0000000

1. INTRODUCTION

From the systematic collection of handprints in 19th century India (Komarinski 2004), the field of biometrics has evolved substantially, encompassing such far-reaching modalities as: fingerprints (Jain, et al. 1999), head dimensions (Harmon, et al. 1981), iris patterns (Daugman 2004), and face geometry (Wiskott, et al. 1997). While the biometric field has grown far beyond its humble roots, the above-mentioned techniques are not without their flaws, and many are prone to exploitation by falsified features (Williams 2002). This has lead to the present need for biometric techniques that are not only capable of identifying an individual with high accuracy, but are capable of distinguishing falsified information, often encompassed by the properties of counterfeit-resistance and liveness detection.

The human oculomotor system may be unique in its ability to address these issues, and is already employed in many biometric systems that make use of iris patterns (Daugman 2004), face (Abate, et al. 2007), retina patterns (Jain, et al. 2000), conjunctival vasculature (Crihalmeanu and Ross 2012), periocular information (Park, et al. 2009), eye movements (Kasprowski and Ober 2004), and pupil dilation (Bednarik, et al. 2005). The complex anatomical structure of the human oculomotor system and the dual aspect of physical and neurological components makes the accurate replication of eye movements practically infeasible outside of a living subject, providing inherent liveness detection and theoretically high counterfeit-resistance (Komogortsev and Karpov 2013; Komogortsev, et al. 2012b).

Special gratitude is expressed to Katie Holland for her aid with technical illustrations. This work is supported in part by Texas State University, NSF CAREER Grant #CNS-1250718, NSF GRFP Grant #DGE-11444666, and NIST Grant #60NANB12D234.
Author's address: O. Komogortsev, Texas State University, Department of Computer Science, San Marcos, TX 78666; email: ok11@txstate.edu; C. Holland, Texas State University, Department of Computer Science, San Marcos, TX 78666; email: ch1570@txstate.edu; A. Karpov, Texas State University, Department of Computer Science, San Marcos, TX 78666; email: ak26@txstate.edu; L. Price, Texas State University, San Marcos, TX 78666; email: lp11@txstate.edu.

DOI:http://dx.doi.org/10.1145/0000000.0000000

1.1 Human Oculomotor System

The oculomotor plant, shown in Figure 1, encompasses the primary physical components of the human oculomotor system (Wilkie 1970), and is composed of the eye globe, six extraocular muscles, surrounding tissues, and various ligaments, tendon-like components, and liquids. Extraocular muscles include: the lateral and medial recti, responsible for horizontal rotation; the superior and inferior recti, responsible for vertical rotation; and the superior and inferior obliques, responsible for torsional rotation.

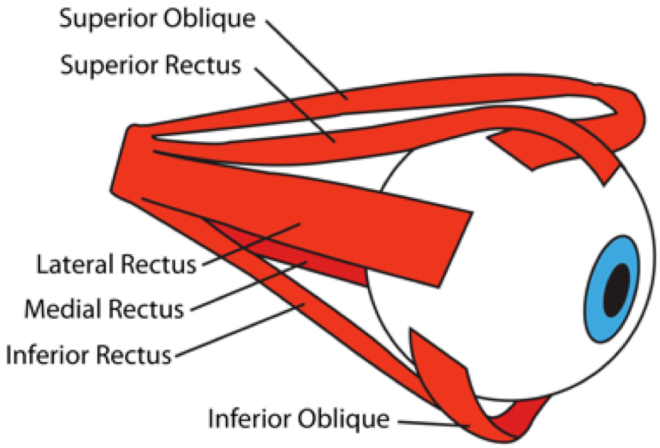

Figure 1. The oculomotor plant.

When considered as a cohesive system, each component adds specific properties to the mechanics of the whole (Leigh and Zee 2006). The extraocular muscles provide the forces required to rotate the eye globe, with opposing muscle pairs performing mutually exclusive roles of agonist (AG) and antagonist (ANT), where the agonist muscle contracts and pulls the eye globe and the antagonist muscle expands to resist the pull. Each extraocular muscle is composed of both thin and thick filaments that cause a strict dependence between the force exerted by a muscle and its length/velocity of contraction. The eye globe provides inertia to the system, along with the resistive properties of the surrounding tissue and ligaments (Komogortsev and Khan 2008).

The brainstem control describes the complex network of neurological components that signal the extraocular muscles to expand and contract (Leigh and Zee 2006). It should be noted that the term brainstem control is based on early modeling of the human oculomotor system, whereas eye movements are generated by components throughout the brain, not isolated to the brainstem itself. These components include sub-regions of the thalamus, superior colliculus, and posterior parietal cortex (Duchowski 2007), where: the thalamus is responsible for engaging visual attention; the superior colliculus is responsible for relocating visual attention; and the posterior parietal cortex is responsible for disengaging visual attention. These interconnected systems are ultimately responsible for the many and varied types of human eye movement. The brainstem control produces a signal that corresponds to the desired type, direction, and magnitude of eye movement, and the oculomotor plant responds, enacting the mechanical functions that produce the desired movement.

The oculomotor plant, driven by the neuronal control signal, primarily exhibits six eye movement types described in detail by (Leigh and Zee 2006), these include: fixations, saccades, smooth pursuits, optokinetic reflex, vestibule-ocular reflex, and vergence. Fixation occurs when the eye globe is held in a relatively stable position to provide visual acuity on a fixed point; saccades occur when the eye globe rotates rapidly between points of fixation, with little visual acuity maintained during rotation; smooth pursuit occurs when the eye globe rotates slowly, maintaining fixation on a slowly moving point; optokinetic reflex refers to the sequence of smooth pursuit and saccadic eye movements which occur when the eye attempts to maintain a fixation on a rapidly moving point; vestibulo-ocular reflex refers to the corrective eye movements which occur to maintain a fixation on a stationary point during head movement; and, vergence refers to the corrective eye movements which occur to maintain a fixation on a point whose distance changes, without horizontal or vertical motion in the visual field. Of these, fixations and saccades are of particular interest in the field of human-computer interaction, as they are simple and easy to evoke, measure, and identify on a stationary screen. These eye movements are affected not only by the physical structure of the oculomotor plant, but also by frequency characteristics of the neuronal control signal and its speed of propagation.

1.2 Previous Research

The foundations of eye movement-related biometrics stem from the early work of (Noton and Stark 1971), in defining a branch of study known as scanpath theory. The term scanpath refers to the spatial path formed by a sequence of fixations and saccades. In 1971, Noton and Stark found that the scanpath formed by a subject during the initial viewing of a pattern was repeated in 65% of subsequent viewings. Further, the scanpath formed for a given stimulus pattern tends to vary from person to person (Noton and Stark 1971; Rayner 1998; Schnitzer and Kowler 2005). These properties provide a basis for the use of eye movements as a biometric.

To our knowledge, (Kasprowski and Ober 2004) was the first to investigate the viability of eye movements in a biometric context. In doing so, they considered the first 15 cepstral coefficients of the gaze position across each recording, a technique commonly applied to speech recognition (Jain, et al. 2007). Information fusion was applied by naïve Bayes, C4.5 decision trees, SVM polynomial, and k-nearest neighbor (k = 3 and 7). The best reported results provided 1% average false acceptance rate and 29% average false rejection rate over 10-fold stratified cross validation.

(Silver and Biggs 2006) followed, investigating higher-level eye movement features in conjunction with keystroke biometrics, including: the 8 most significant fixations, fixation count, average fixation duration, average saccade

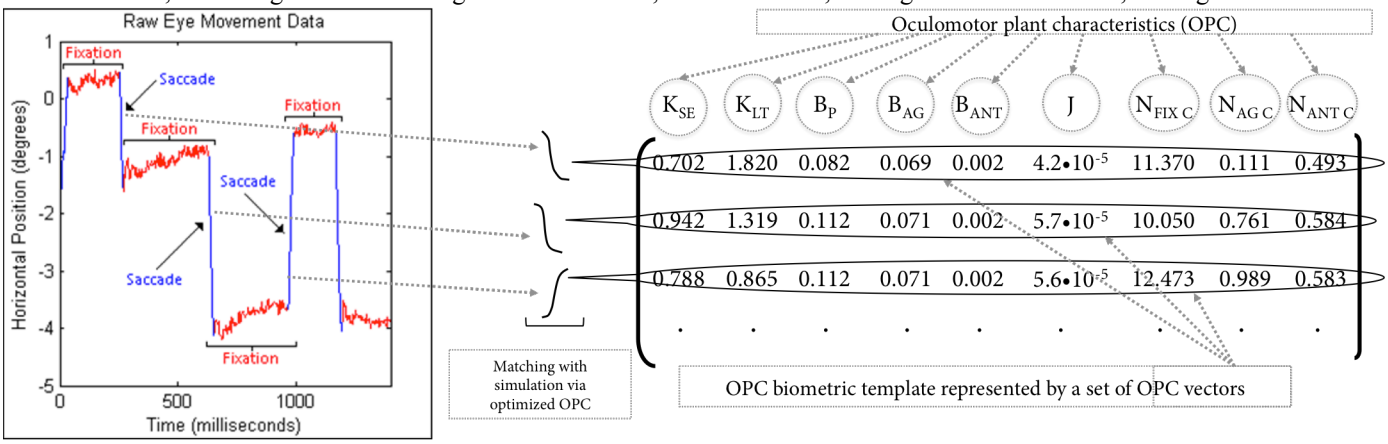

Figure 2. Eye movement signal with classified fixations and saccades (left); 9-parameter oculomotor plant model biometric template (right).

velocity, average saccade duration, and average vertical position. Features were combined using a neural network, and provided 66% true positive percentage and 98% true negative percentage on the considered dataset.

(Holland and Komogortsev 2011) considered individual and aggregated scanpath properties, including: fixation count, average fixation duration, average vectorial saccade amplitude, average horizontal saccade amplitude, average vertical saccade amplitude, average vectorial saccade velocity, average vectorial saccade peak velocity, velocity waveform indicator (Q), scanpath length, scanpath area, regions of interest, inflection count, amplitude-duration coefficient, and amplitude-peak velocity coefficient. Features were compared with a Gaussian kernel and combined by weighted average, achieving a 27% equal error rate.

Most recently, (Rigas, et al. 2012) evaluated the use of graph-based matching across the gaze position of each recording, comparing minimum spanning trees using the multivariate Wald-Wolfowitz runs test. These techniques achieved a 30% equal error rate and 70% rank-1 identification rate.

1.3 Motivation & Hypothesis

We hypothesize that the anatomical characteristics of the human eye may be accurately estimated from the properties of saccadic eye movements, and that these oculomotor plant characteristics may be utilized to uniquely identify individuals in a biometric context.

In previous work, Komogortsev et al. examined the feasibility of the proposed techniques under a verification scenario using a fixed, high-resolution dataset (Komogortsev, et al. 2012c). The current paper expands greatly on previous work, adding: random selection of training and testing partitions; biometric error rates under both verification and identification scenarios; performance comparison on a low-resolution dataset; an extended 18-parameter oculomotor plant model; an in-depth statistical analysis of model parameters; and a comparison to the biometric performance of the 9-parameter oculomotor plant model.

2. OCULOMOTOR PLANT CHARACTERISTICS

In this work, we build on the methods proposed by (Komogortsev, et al. 2012c). To perform biometrics via oculomotor plant characteristics (OPC), a mathematical model of the oculomotor plant simulates saccadic trajectories and compares them to the recorded trajectory extracted from the gaze position across each saccade. The computed differences trigger OPC estimation procedures, which attempt to find optimal OPC values that minimize the

difference between the recorded and simulated trajectories. Optimized OPC values form a biometric template that can be employed for biometric verification and identification, as shown in Figure 2.

2.1 Oculomotor Plant Model

The goal of the oculomotor plant model is to describe a system of equations capable of accurately reproducing the characteristics of normal human eye movements in real-time, while accounting for the unique properties of the extraocular muscles responsible for rotation of the eye globe. From these equations, the hidden and unobservable muscle properties specific to an individual (similar to a fingerprint) could be determined programmatically from the measurable properties of eye movements. A number of models have been proposed by various sources (Quaia and Optican 2003), generally representing the oculomotor plant linearly in one-dimension (horizontal) or non-linearly in three dimensions (horizontal, vertical, torsional).

In the current work, we employ a two-dimensional linear homeomorphic model of the oculomotor plant as developed by (Komogortsev, et al. 2012a; Komogortsev and Jayarathna 2008). The considered model is driven by twelve differential equations, and is capable of simulating saccades with properties resembling normal humans (Komogortsev, et al. 2012a) on a two-dimensional plane (horizontal and vertical). Advantages of the considered model include: major anatomical components are accounted for and can be estimated; linear representation simplifies the parameter estimation process, while producing accurate simulation data within the bounds of a computer monitor; the architecture of the model allows separation into two one-dimensional models of the form described by (Komogortsev and Khan 2008), providing for concurrent execution during parameter estimation and eye movement simulation. The 9- and 18-parameter models described in the following sub-sections are one-dimensional models containing the corresponding physical parameters to simulate each component of movement – vertical or horizontal. For information on the use of one-dimensional models to simulate two-dimensional movement, please refer to (Komogortsev, et al. 2012a).

2.2 Oculomotor Plant Characteristics

We refer to the parameters of the oculomotor plant model as oculomotor plant characteristics (OPC). These parameters describe important physical and neurological properties exhibited by the system. Each extraocular muscle exhibits: series elasticity, the resistive properties of a muscle, associated with tendons, while the muscle is innervated by the neuronal control signal; length-tension relationship, the relationship between the length of a muscle and the force it is capable of exerting; force-velocity relationship, the relationship between the velocity of muscle expansion/contraction and the force it is capable of exerting; tension slope and tension intercept, which dictate the reaction of the muscle to innervation and ensure equilibrium during fixation, respectively. As well, the inertial mass of the eye globe and passive viscosity of the surrounding tissue must be taken into account.

The considered model employs a pulse-step representation of the neuronal control signal, in which the neural step indicates the magnitude of the neural signal during fixation, the neural pulse indicates the magnitude of the neural signal during saccade, and the pulse width indicates the duration of the neural pulse. Activation and deactivation time describe the time required for changes in the neuronal control signal to propagate through the extraocular muscles.

2.3 Oculomotor Plant Model (9-Parameter)

The 9-parameter oculomotor plant model simplifies certain assumptions of the model by employing fixed constants in the estimation of the neuronal control signal as depicted by the equations in Section 2.5.2 of (Komogortsev and Khan 2008). As a result, a variable parameter vector for the following oculomotor plant characteristics is estimated by the process described by (Komogortsev, et al. 2012c), with each entry followed by notation and initial value:

1. *Series Elasticity* [K_{SE} = 2.5 g/°]
2. *Length-Tension Relationship* [K_{LT} = 1.2 g/°]
3. *Force-Velocity Relationship* (AG) [B_{AG} = 0.046 g•s/°]
4. *Force-Velocity Relationship* (ANT) [B_{ANT} = 0.022 g•s/°]
5. *Passive Viscosity* [B_P = 0.06 g•s/°]
6. *Tension Slope* (Agonist) [N_{AG_C} = 0.8 g]
7. *Tension Slope* (Antagonist) [N_{ANT_C} = 0.5 g]
8. *Inertial Mass* [J = 0.000043 g•s^2/°]
9. *Tension Intercept* [N_{FIX_C} = 14.0 g]

2.4 Oculomotor Plant Model (18-Parameter)

The 18-parameter oculomotor plant model includes all components of the 9-parameter model, with a few additions and modifications. Of particular note: the series elasticity and length-tension parameters are split into agonist and antagonist counterparts; muscle activation/deactivation time constants that convert the neuronal control signal to activate state tension are added to the model; and additional non-fixed parameters are added for neural pulse magnitude and duration. The expanded model produces a variable parameter vector for the following oculomotor plant characteristics, with each entry followed by notation and initial value:

1. *Series Elasticity* (AG) [$K_{AG\_SE} = 2.5$ g/°]
2. *Series Elasticity* (ANT) [$K_{ANT\_SE} = 2.5$ g/°]
3. *Length-Tension Relationship* (AG) [$K_{AG\_LT} = 1.2$ g/°]
4. *Length-Tension Relationship* (ANT) [$K_{ANT\_LT} = 1.2$ g/°]
5. *Force-Velocity Relationship* (AG) [$B_{AG} = 0.046$ g•s/°]
6. *Force-Velocity Relationship* (ANT) [$B_{ANT} = 0.022$ g•s/°]
7. *Passive Viscosity* [$B_P = 0.06$ g•s/°]
8. *Tension Slope* (AG) [$N_{AG\_C} = 0.8$ g]
9. *Tension Slope* (ANT) [$N_{ANT\_C} = 0.5$ g]
10. *Inertial Mass* [$J = 0.000043$ g•s^2/°]
11. *Activation Time* (AG) [$\tau_{AG\_AC} = 11.7$]
12. *Activation Time* (ANT) [$\tau_{ANT\_AC} = 2.4$]
13. *Deactivation Time* (AG) [$\tau_{AG\_DE} = 2.0$]
14. *Deactivation Time* (ANT) [$\tau_{ANT\_DE} = 1.9$]
15. *Tension Intercept* [$N_{FIX\_C} = 14.0$ g]
16. *Neural Pulse* (AG) [$N_{AG\_SAC} = 55$ g]
17. *Neural Pulse* (ANT) [$N_{ANT\_SAC} = 0.5$ g]
18. *Neural Pulse Width* [PW = § ms]

All neural pulse width (§) values between 6 milliseconds and the duration of the saccade were examined. (Komogortsev and Khan 2008) provide further description of each OPC parameter. Parameters for both the 9- and 18-parameter models correspond to the matrix equations described in Section 3.2 of (Komogortsev, et al. 2012c).

2.5 Estimation of Oculomotor Plant Characteristics

In order to estimate oculomotor plant characteristics for a given saccade, the model is initialized with default parameters based on the relevant literature (Bahill 1980; Komogortsev and Jayarathna 2008; Komogortsev and Khan 2008). An error function is defined as the absolute difference between the measured and simulated eye movement trajectory. Several forms of error function were tested during early investigation, and according to empirical observation the absolute difference provided an advantage over other estimations such as root mean squared error (RMSE) due to its higher absolute sensitivity to the differences in trajectory.

The Nelder-Mead simplex algorithm (Lagarias, et al. 1998) is used to estimate model parameters that minimize the error function. Lower and upper boundaries are imposed to prevent reduction or growth of each parameter to values less than 10% or greater than 1000% of its default value. Stability degradation of the numerical solution for the differential equations describing the model is used as an additional indicator for acceptance of the suggested parameter values by the estimation algorithm.

3. METHODOLOGY

Previous research has shown that minor variations in eye tracking specifications, such as spatial accuracy and temporal resolution, can have a substantial impact on the biometric viability of eye movements (Holland and Komogortsev 2012). Therefore, to properly evaluate the proposed techniques, it was deemed necessary to examine biometric accuracy on both high- and low-resolution eye-tracking systems. The considered scenarios present two extreme cases (small subject pool, high-quality recording equipment and large subject pool, low-quality recording equipment) from which it is possible to show the performance of the proposed biometric methods. Biometric performance results, presented in Section 4, were measured on existing eye movement datasets, collected by (Komogortsev 2012a; Komogortsev 2012b) and openly available online, with collection methodology presented in the following subsections.

3.1 Apparatus & Software

High-resolution eye movements were recording using an EyeLink 1000 eye tracking system, with a temporal resolution of 1000 Hz, vendor-reported spatial accuracy of 0.5°, average calibration accuracy of 0.7° (SD = 0.5°), and average data validity of 98.3% (SD = 1.7%). Stimuli were presented on a flat screen monitor positioned at a distance of 685 mm from each subject, with dimensions of 640×400 mm, and screen resolution of 2560×1600 pixels.

Low-resolution eye movements were recorded using a modified version of the open-source ITU Gaze Tracker software (Agustin, et al. 2009) and PlayStation Eye Camera, with a temporal resolution of 75 Hz and average calibration accuracy of 1.1° (SD = 0.8°). The PlayStation Eye Camera is roughly equivalent to, and may easily be substituted by, an inexpensive webcam. Average data validity is unreportable as it was not possible to detect when the eye tracker began tracking an area of the image other than the subject pupil (i.e. rim of glasses, eyelashes, hair, etc.). Stimuli were presented on a flat screen monitor positioned at a distance of 540 mm from each subject, with dimensions of 375×302 mm, and screen resolution of 1280×1024 pixels.

A chin rest was employed to improve stability. SVMlight, an open source implementation of the Support Vector Machine (Vapnik 1999), was utilized for SVM-based fusion, all other algorithms and analysis were implemented and performed in MATLAB, and run using a 3.1 GHz quad-core CPU with 16 GB memory.

3.2 Participants

High-resolution eye movement data was collected for a total of 32 subjects (26 males, 6 females), ages 18 – 40 with an average age of 23 (SD = 5.4). 29 of the subjects performed 4 recording each, and 3 of the subjects performed 2 recordings each, generating a total of 122 unique eye movement recordings. Subjects were given a 20-minute break between the 1st and 2nd recording, 1-2 weeks between the 2nd and 3rd recording, and 20 minutes between the 3rd and 4th recording.

Low-resolution eye movement data was collected for a total of 172 subjects (116 males, 56 females), ages 18 – 49 with an average age of 23 (SD = 5.3). 171 of the subjects performed 2 recordings each, and 1 of the subjects performed 1 recording, generating a total of 343 unique eye movement recordings. There was a 15-minute time difference between the 1st and 2nd recording.

3.3 Procedure

Data collection procedures were equivalent for both eye-tracking systems, and there was no overlap in the subject pools of the two datasets. Each subject generated eye movement recordings over multiple sessions for a single stimulus. The stimulus employed a technique commonly used to evoke a fixed-amplitude saccade at regular intervals (Leigh and Zee 2006). A single white dot jumped back and forth on a plain black background, eliciting a 30° horizontal saccade with each jump. These distances were chosen due to screen constraints, and the complications associated with separating low-amplitude saccades (less than 1°). Subjects were instructed to follow the white dot with their eyes, with 100 saccades elicited for each recording session, and a 1 second fixation duration between saccades, for a data collection time of 100 seconds per recording.

Eye movement recordings were parsed and processed to remove invalid data points (often caused when the subject blinks or looks away from the screen), with average data validity for the high- and low-resolution recordings provided in Section 3.1. Recordings were stored in an eye movement database, with each record linked to the stimulus, subject, and session that generated the recording. The recordings were then processed and classified into fixations and saccades using an eye movement classification algorithm (Salvucci and Goldberg 2000).

A velocity threshold algorithm (I-VT) with documented accuracy (Komogortsev, et al. 2010) was employed to classify individual data points with a velocity greater than 70°/sec as belonging to a saccade, with all remaining points belonging to fixations. A comparatively high classification threshold was chosen to reduce the impact of trajectory noise near the beginning and end of each saccade. Saccades of less than 4° amplitude, duration less than 20 milliseconds, or containing abnormal trajectory artifacts were discarded. OPC parameters were estimated for each remaining saccade according to the techniques described in Section 2.

Eye movement recordings were partitioned into training and testing sets, by subject, according to a uniformly random distribution; such that, all recordings from half of the subject pool of a given dataset appeared in the training set, with the other half of the subject pool in the testing set, and there was no subject overlap between training and testing. Error rates were calculated under biometric verification and identification scenarios for 20 random partitions of training and testing sets. Regression was performed on the error rates achieved across all partitions to generate receiver operating characteristic (false acceptance rate vs. true positive rate) and cumulative match characteristic (rank

vs. identification rate) curves, with $R^2 > 0.9$ in all cases. Equal error rate, rank-1 identification rate, and area-under-curve were calculated from the regression.

Biometric match scores were generated comparing OPC parameters between pairs of recordings. Hotelling's T-square test (abbreviated as Hotelling T^2 in the remainder of the manuscript) was used to compare across all OPC parameters (Hotelling 1931) and the two-sample Cramér-von Mises test was used to compare individual OPC parameters. In the latter case, match scores were generated for each OPC parameter, and information fusion was applied by weighted mean, likelihood ratio (Nandakumar, et al. 2008), linear support vector machine (Cortes and Vapnik 1995), and 50-tree random forest (Breiman 2001), with algorithm parameters selected on the training set. Error rates were then calculated on the testing set for individual matches and fusion techniques under biometric verification and identification scenarios.

4. RESULTS

Prior to conducting statistical tests of between subject differences based on 9- and 18-parameters, the data were evaluated for the general linear model assumptions of (1) homogeneity of variance between and within subjects using Bartlett's test of homogeneity of variance (Bartlett 1937), (2) the type of autoregressive process of parameters measured within subjects over time (i.e. change in the estimated OPC vectors with each new processed saccade), and (3) screening the parameters for normality of the distributions. In the case where parameter distributions were statistically skewed (e.g., 95% of the parameters), we used a logarithmic transformation.

The results of these diagnostic tests revealed that the variance of OPC vectors within subjects were highly unstable over time. A highly similar pattern was observed between subjects relative to the within subjects variation over time. Further diagnostics revealed that the initial 40 OPC vectors captured from the first 40 saccades counted from the beginning of the eye movement data collection process had higher stability of the variance than the remainder of the OPC vectors extracted from all subsequent saccades. This phenomenon possibly indicates the impact of drifting, eye tracking equipment slippage, and/or subject fatigue that might occur in case of the prolonged data capture. However, this pattern in the variance of the OPC data was inconsistent across subjects, therefore we worked with all measurements provided by the data capture in the 9- and 18-parameter models.

4.1 Model Complexity

The OPC estimated by each model displayed statistically significant departures from normality (i.e. skewness and kurtosis). To correct for statistically significant departures of skewness and kurtosis, parameter values were transformed using a logarithmic transformation prior to statistical analyses. In our study, the logarithmic transformation of parameters yielded greater conformity to the normal distribution (a requirement of parametric statistical hypothesis tests) and increased statistical power relative to any subsequent statistical tests (e.g., the Hotelling's T^2 test).

To determine which model (i.e. the 9- vs. 18-parameter) was superior in terms of explaining unique parts of the variance accounted for by each of the OP models, a series of principal component analyses were conducted. There is no single statistical measure that provides conclusive evidence that one principal component analysis solution is superior to another. Therefore, two techniques/criteria were used to statistically compare the 9- and 18-parameter models in order to determine superiority of a model specific to our research goals (Tabachnick and Fidell 2006).

The first criteria involved evaluating the percentage of variance accounted for by a component based on the eigenvalues (i.e. an optimal linear combination of parameters compressed into a single value) in the 9- and 18-parameter models; we applied a target value of total or cumulative variance accounted for > .95. Additionally, the pattern of variance allocation across parameters was examined (e.g., what percentage of variance does each component explain in relation to the total number of components) (Hair, et al. 1998).

The second criteria included an evaluation of the reproduced correlation matrix to inspect the pattern and magnitude of the residuals. Conducting a principal component or factor analysis involves comparing a correlation matrix based on the observed (empirical) data to a correlation matrix implied by a theoretical model (e.g., in our study the 9- and 18-parameter models across different resolutions). A residual analysis serves to evaluate the degree to which the empirical correlation matrix matches or aligns with a theoretical model.

Results of these statistical techniques revealed that the 18-parameter model at resolutions of 75 Hz and 1000 Hz yielded a more complete explanation of the variance across the parameters than did the 9-parameter model. For example, in the 75 Hz 18-parameter model, at eigenvalue number 17 out of 18, over 3.5% of the total variance was explained. In the 1000 Hz data, at eigenvalue number 17 out of 18, 1.86% of the variance was explained. Conversely,

in the 75 Hz 9-parameter model, at eigenvalue number 9 out of 9, only 2.4% of the variance was explained, and in the 1000 Hz data, at eigenvalue 9 out of 9, only 1.4% of the variance was explained.

A statistical artifact of model fitting and linear optimization techniques such as PCA is that by adding more parameters improves model-data fit; however, in certain circumstances the improved fit may not yield practically useful information given the context of a particular model or the overall goal of an investigation. Nevertheless, our goal in using PCA was to estimate the proportion of variance explained by each parameter within each model, so as to better understand the relative contribution of each parameter within the 9- and 18-parameter models. In this vein, the use of PCA was exploratory and serves to increase understanding of the two models.

This descriptive pattern of component solutions across resolution and parameter complexity revealed that the 18-parameter model explains finer pieces of the system than does the 9-parameter model. A residual analysis of the reproduced correlation matrices of the 9- and 18-parameter models at both resolutions revealed smaller values (i.e. no residuals exceeded .001) for the 18-parameter model, indicating superiority of the 18-parameter model to the 9-parameter model. The 9-parameter model displayed a higher MSA value (.32) measure of sampling adequacy than did the 18-parameter model (.09); this pattern is reversed from our previous analyses, but is not statistically important relative to the PCA.

4.2 Biometric Match Scores

During our initial investigation of these techniques, several statistical tests were considered for comparing the distribution of oculomotor plant characteristics attributed to a given subject. Considered tests included the: two-sample Cramér-von Mises test, two-sample Kolmogorov-Smirnov test, Ansari-Bradley test, Mann-Whitney U-test, two-sample F-test, and two-sample t-test. Of these, the two-sample Cramér-von Mises test provided the least biometric error, followed closely by the two-sample Kolmogorov-Smirnov test. In general, the Ansari-Bradley test, Mann-Whitney U-test, two-sample F-test, and two-sample t-test performed poorly due to the fact that they make certain assumptions about the underlying distributions.

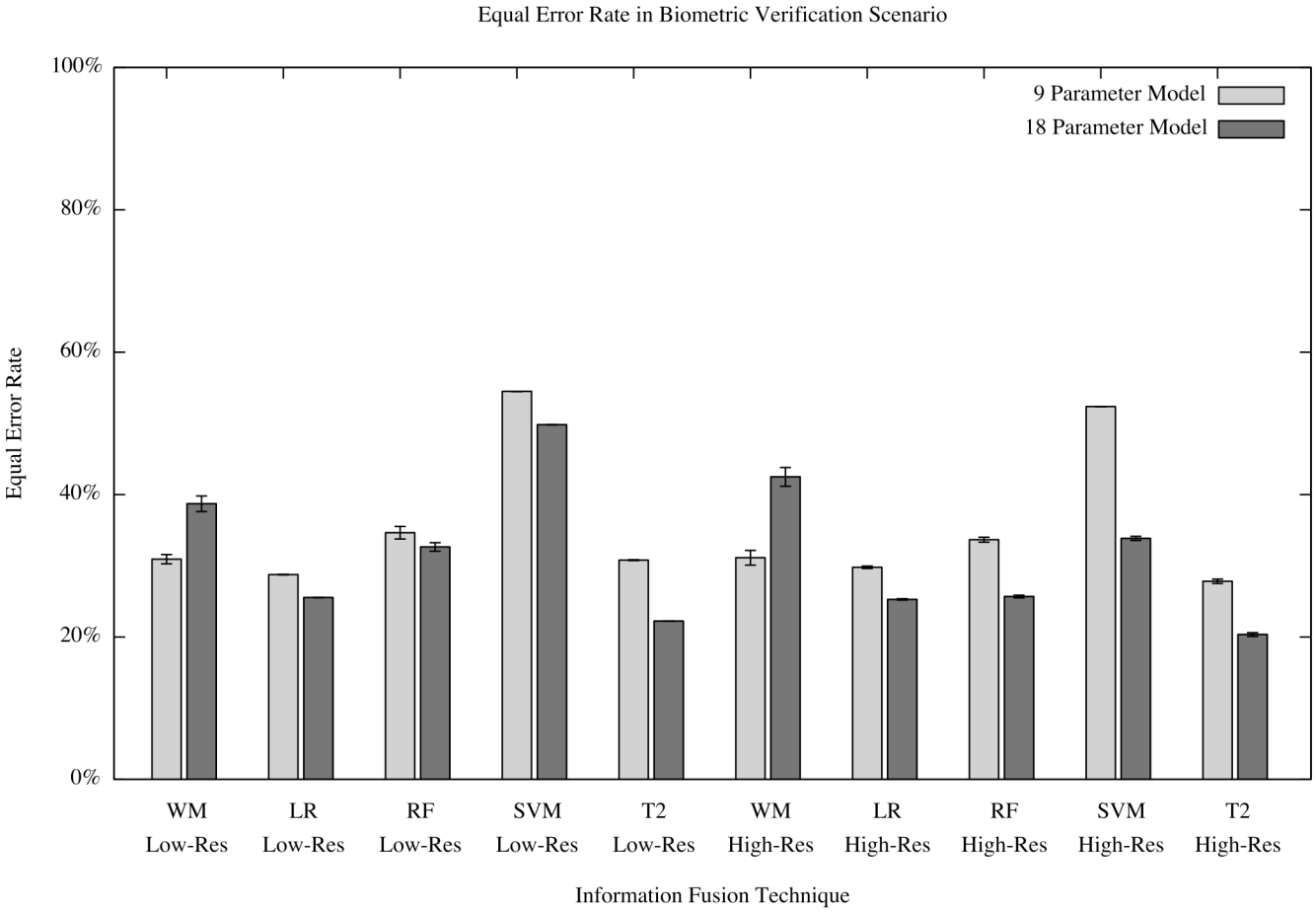

Figure 3. Comparative equal error rates in a biometric verification scenario. Error bars indicate 95% confidence interval. WM = Weighted Mean; LR = Likelihood Ratio; RF = Random Forest; SVM = Support Vector Machine; T2 = Hotelling T^2

To assess the stability of biometric matching, Kolmogorov-Smirnov tests for uniformity and normality and Wald-Wolfowitz runs tests for randomness were applied to the match scores generated for each OPC using the two-sample Cramér-von Mises test. The results indicate that biometric match scores are highly non-random, in that they do not conform to normally or uniformly distributed random sequences ($p < 0.0001$) and do not contain random sub-sequences ($p < 0.0001$).

Shannon entropy was calculated for match scores to assess the information density of individual OPC. Low Shannon entropy (minimum = 0) indicates clustering of match scores around specific values, while high Shannon entropy (maximum = 8) indicates that the produced match scores are more unique and tend to fall within the range of possible values, rather than at the extremes. With the exception of neural pulse width, match scores for OPC parameters ranged between Shannon entropy of 4.9 – 7.9 (mean = 6.8 ± 0.9), indicating a relatively even spread of match scores within the range. In the case of neural pulse width, Shannon entropy reaches a low of 2.8, indicating that match scores cluster around specific values. This is not unexpected, as the values for neural pulse width are limited to integer values less than the duration of the saccade, which leads to saccades from different subjects sharing similar neural pulse properties despite differences in muscle properties.

The decidability index (or d-prime) of match scores is a measure of the separation of two distributions, and may be applied to the distributions of genuine and imposter match scores as a measure of achievable error rate tradeoff. Decidability index assumes a Gaussian distribution of match scores, which is often the case; however, the genuine and imposter match scores generated for each OPC fail to conform to a Gaussian distribution, leading to particularly low decidability indices in the range of 0.01 – 0.27 (mean = 0.07 ± 0.05).

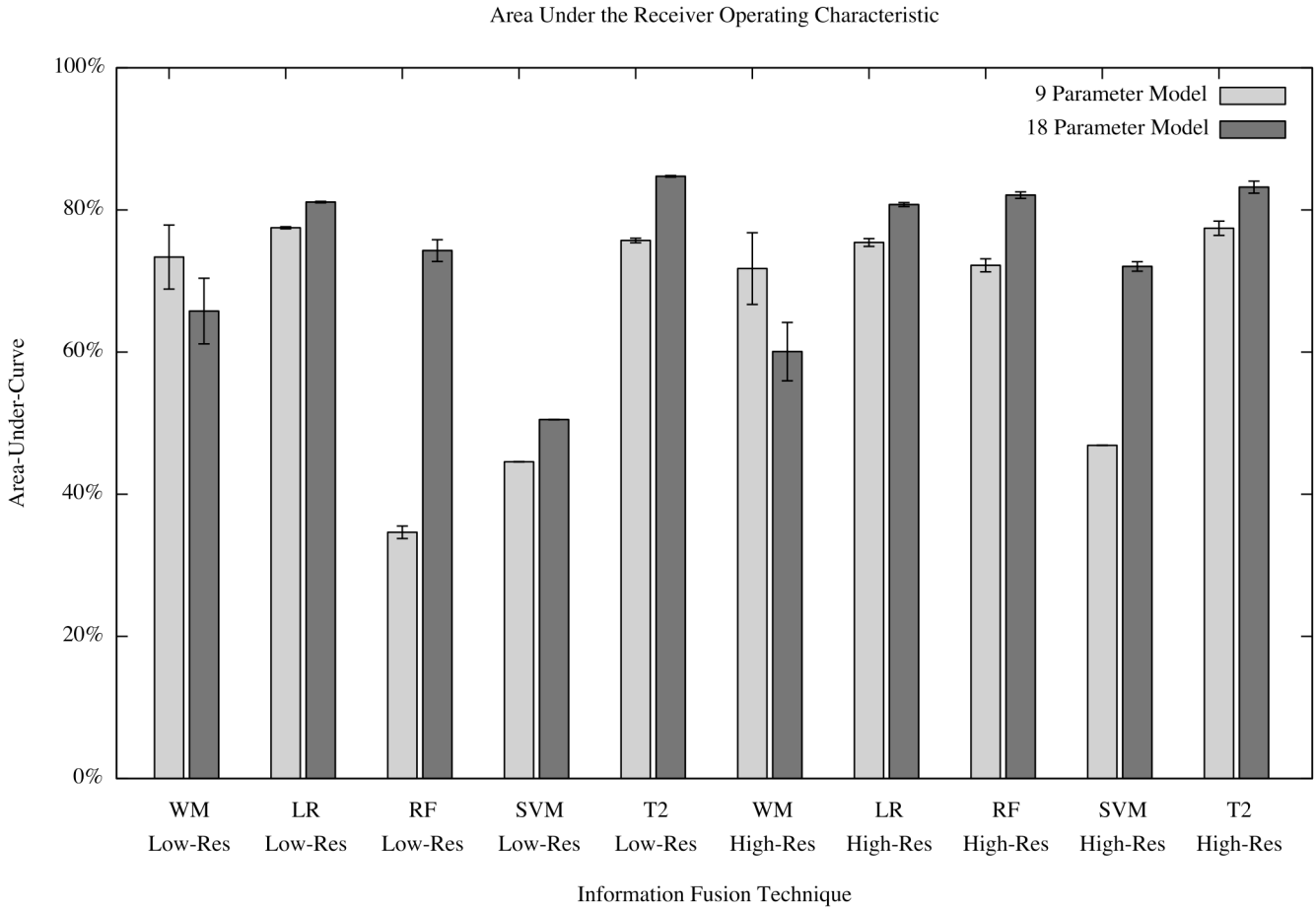

Figure 4. Comparative area-under-curve in a biometric verification scenario. Error bars indicate 95% confidence interval. WM = Weighted Mean; LR = Likelihood Ratio; RF = Random Forest; SVM = Support Vector Machine; T2 = Hotelling T^2

4.3 Biometric Accuracy

Biometric verification involves comparing each record in the testing set against every other record in the testing set exactly once. False acceptance rate is defined as the rate at which imposter match scores exceed the acceptance threshold, false rejection rate is defined as the rate at which genuine match scores fall below the acceptance threshold, and true positive rate is defined as the rate at which genuine match scores exceed the acceptance threshold. The equal error rate, shown in Figure 3, indicates the common value at which the proportion of false positives is equal to the proportion of false negatives. The receiver operating characteristic (ROC) plots true positive rate against false acceptance rate, and the area-under-curve of the ROC, shown in Figure 4, provides a metric by which to compare the accuracy achieved by ROC curves, where 100% AUC indicates perfect accuracy.

Biometric identification involves comparing every record in the testing set against every other record in the testing set. Identification rate is defined as the rate at which enrolled subjects are successfully identified as the correct individual, where rank-*k* identification rate is the rate at which the correct individual is found within the top *k* matches. Hence, the rank-1 identification rate, shown in Figure 5, is the rate at which the correct individual has the highest match score. The cumulative match characteristic (CMC) plots identification rate by rank, for all ranks, and the area-under-curve of the CMC, shown in Figure 6, provides a metric by which to compare the accuracy achieved by CMC curves, where 100% AUC indicates perfect accuracy.

Match scores for individual OPC are combined for a particular subject-to-subject comparison using a technique referred to as information fusion. Information fusion can occur at the feature- or the match score-level. In this paper,

we consider one type of feature-level fusion, the Hotelling T^2 test, and four types of match-score level fusion: weighted mean, likelihood ratio, random forest, and linear support vector machine. Feature-level fusion makes direct

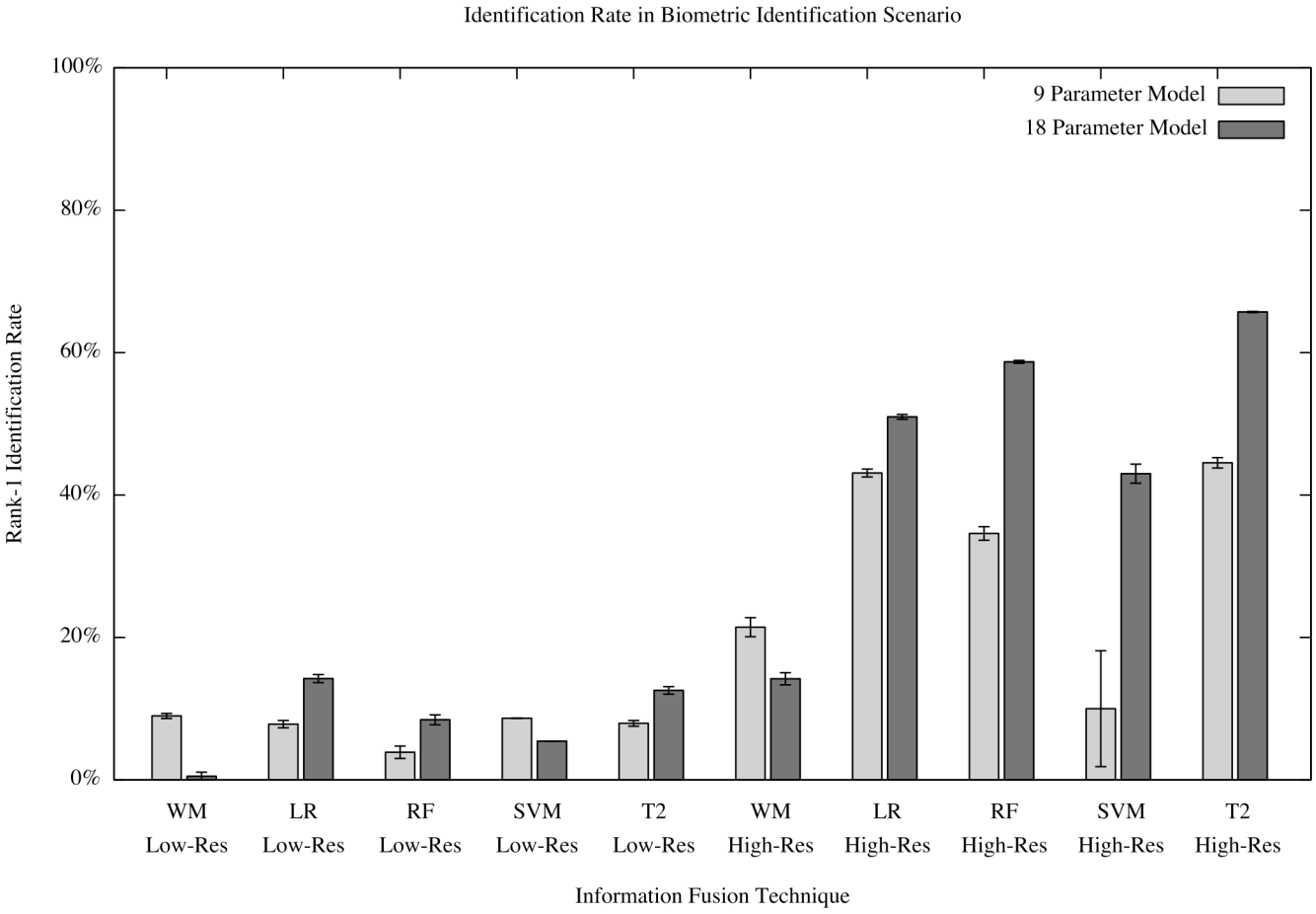

Figure 5. Comparative rank-1 identification rates in a biometric identification scenario. Error bars indicate 95% confidence interval. WM = Weighted Mean; LR = Likelihood Ratio; RF = Random Forest; SVM = Support Vector Machine; T2 = Hotelling T^2

use of OPC values, while match-score level fusion makes use of the match scores generated by a Cramér-von Mises comparison of OPC values.

Of the considered techniques, the Hotelling T^2 test performed better than any combination of individual OPC characteristics (as compared by the two-sample Cramér-von Mises test), achieving both the lowest equal error rate of 20.3% and the highest rank-1 identification rate of 65.7%. Interestingly, the linear support vector machine performed worst of the considered fusion techniques, achieving the highest equal error rate of 54.5%, indicating that the genuine and imposter match scores generated for OPC characteristics are not linearly separable within a hyperplane (supported by the low decidability index of match scores). Of the fusion techniques applied to the Cramér-von Mises comparison of OPC, likelihood ratio-based fusion performed with the most stability, providing the highest rank-1 identification rates on high-resolution 9-parameter model and the low-resolution 18-parameter model, and the lowest equal error rates in all cases.

In considering biometric performance, the 18-parameter oculomotor plant model provides much greater accuracy than the 9-parameter model. This is apparent on both the high- and low-resolution datasets. Considering the best-performing fusion technique, the Hotelling T^2 test, the 18-parameter model provided an: equal error rate improvement of 40% on the high-resolution dataset; equal error rate improvement of 41% on the low-resolution dataset; rank-1 identification rate improvement of 47% on the high-resolution dataset; and rank-1 identification rate improvement of 63% on the low-resolution dataset. It is particularly interesting to note that the Hotelling T^2 comparison of 18-

parameter OPC achieved roughly equivalent equal error rates on both high- and low-resolution datasets (20.3% and 22.2% respectively), though there was an obvious degradation in rank-1 identification rate.

Further, the 18-parameter model outperforms previous applications (Komogortsev, et al. 2012b) of the 9-parameter model, which achieved only 41.7% minimum half-total error rate when applied to horizontal saccades obtained on a high-resolution dataset. It should be noted that the previous dataset made use of different stimuli that

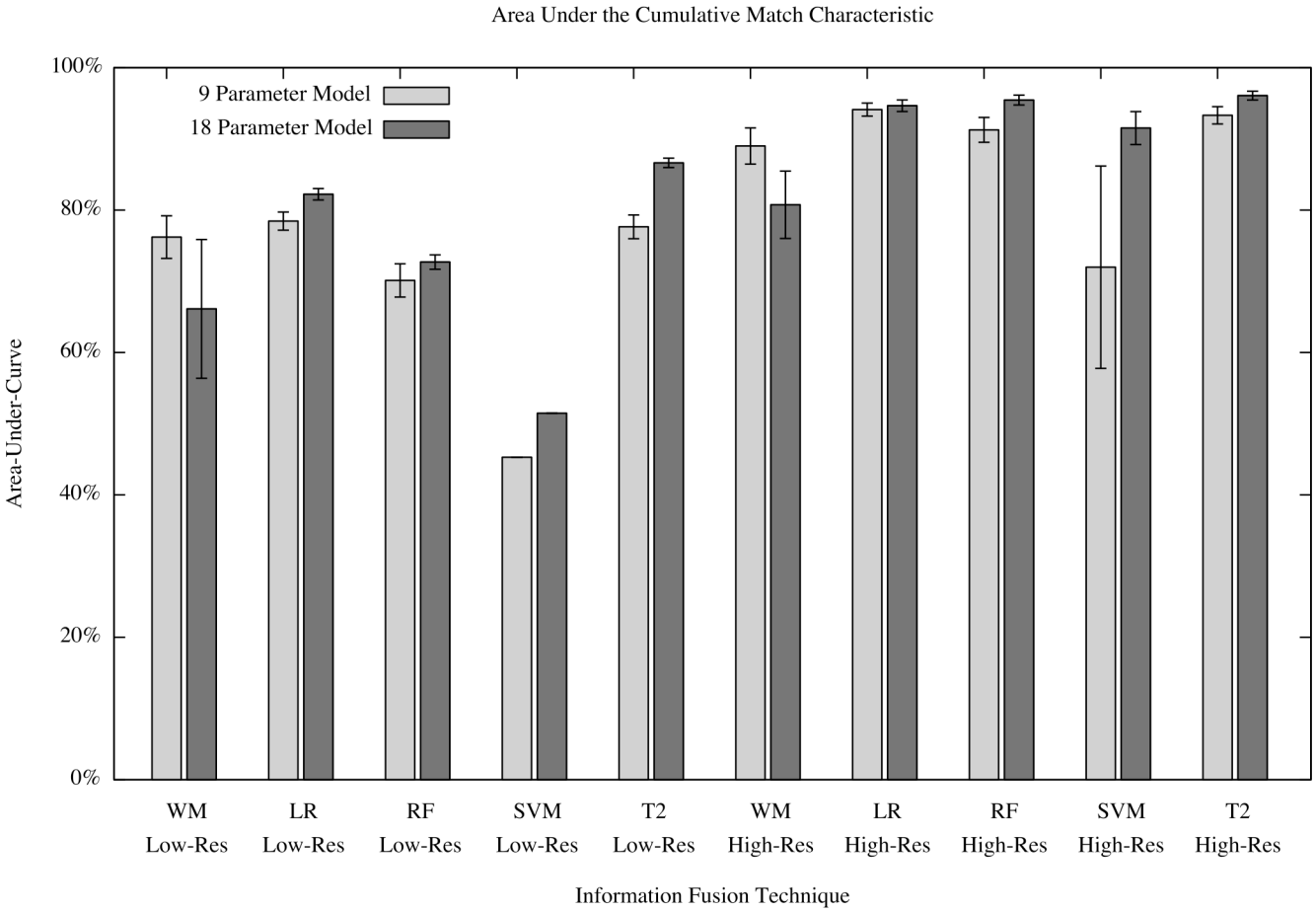

Figure 6. Comparative area-under-curve in a biometric identification scenario. Error bars indicate 95% confidence interval. WM = Weighted Mean; LR = Likelihood Ratio; RF = Random Forest; SVM = Support Vector Machine; T2 = Hotelling T^2

evoked a smaller amount of horizontal saccades, and therefore provided less opportunity for OPC extraction. This may also indicate that the considered techniques are more stimulus dependent than other forms of eye movement biometric (Holland and Komogortsev 2012).

5. FUTURE RESEARCH

The horizontal saccade stimulus employed in this work was purposefully fixed in amplitude, and evoked a large number of saccades. Such fixed experimental parameters allowed us to establish a baseline for the biometric performance of the considered techniques, and the use of a high-resolution commercial eye tracker with fixed head position and controlled lighting provided an environment that was close to ideal; however, additional work is required to understand the biometric performance for saccades of random amplitude, varied spatial placement, and different quantities.

Another area of interest is the parameter estimation speed. The estimation of OPC vectors for each saccade is a slow process, where parameter estimation for a single saccade on the 9-parameter model required, on average, 1500 saccadic simulations, or approximately 15 minutes using a single threaded MATLAB implementation. Despite this,

the employed oculomotor plant model is highly parallelizable, with each saccade trajectory easily processed by a separate thread, and implementation in a lower-level language such as C/C++ may speed up the estimation process. Similarly, a reduction in the number of iterations processed could provide results comparable to those previously obtained.

The linear design of the oculomotor plant model makes it possible to seek analytical solutions to the differential equations that describe the model, thereby providing an opportunity for the direct extraction of OPC from a saccadic trajectory; however, the derivation of an analytical solution is very challenging. Additionally, the investigation of different modeling techniques (of which there are many) might yield a more accurate indication of physical muscle properties (Quaia and Optican 2003).

As well, while these techniques are not yet accurate enough to be useful in a standalone system, less accurate techniques have already been employed to improve the accuracy of multi-modal systems (Komogortsev, et al. 2012b). The ability to seamlessly integrate the proposed techniques with other ocular biometrics (such as iris, retina, and other eye movement biometrics) makes them a solid candidate in this regard. All of these are avenues for future research.

It should be noted that the size of the high-resolution dataset is relatively small; and, although we see similar trends in the low-resolution dataset, an increase in the subject pool of the high-resolution recordings is necessary to guarantee statistical significance. Due to the time and resources required to coordinate large-scale eye movement recording, expansion of the dataset has been deemed an area of future research.

Further, in the current work the time span between recordings was not considered in the randomized splitting of subjects, as we do not consider the span of two weeks to be sufficiently long-term to warrant special consideration. Future research is necessary to identify the effects of template aging, both short- and long-term, on eye movement biometrics.

6. CONCLUSION

This paper has presented an objective evaluation of a novel biometric approach, utilizing the internal, non-visible, anatomical structure of the human eye. The proposed techniques employ a mathematical model of the human eye to estimate physical properties of the system from observable data. The derived properties were evaluated within a biometric framework to determine their efficacy in both verification and identification scenarios.

Based on the results, we conclude that the proposed techniques are at least as effective as existing eye movement biometrics, achieving 20.3% EER and 65.7% rank-1 IR on high-resolution eye tracking equipment, and 22.2% EER and 12.6% rank-1 IR on low-resolution eye tracking equipment. In both cases, the best-achieved results were obtained by comparing across all OPC with the Hotelling T^2 test. Further, we note that the extended 18-parameter model exhibited an obvious improvement in biometric accuracy when compared to the previously considered 9-parameter model. These results bring an interesting perspective in which the authentication accuracy of the OPC method is almost equivalent between a commercial system (costing tens of thousands of dollars) and a common web camera. We hypothesize that this important outcome would strengthen the validity of inexpensive ocular biometrics systems that employ both iris and eye movement biometric traits, as demonstrated by (Komogortsev, et al. 2012b).

REFERENCES

Abate, A. F., Nappi, M., Riccio, D. and Sabatino, G. 2007. 2D and 3D Face Recognition: A Survey. *Pattern Recognition Letters* 28, 14, 1885-1906.

Agustin, J. S., Skovsgaard, H., Hansen, J. P. and Hansen, D. W. 2009. Low-cost Gaze Interaction: Ready to Deliver the Promises. In *Conference on Human Factors in Computing (CHI)*, ACM, 4453-4458.

Bahill, A. T. 1980. Development, Validation, and Sensitivity Analyses of Human Eye Movement Models. *Critical Reviews in Bioengineering* 4, 4, 311-355.

Bartlett, M. S. 1937. Properties of Sufficiency and Statistical Tests. *Proceedings of the Royal Society of London* 160, 901, 268-282.

Bednarik, R., Kinnunen, T., Mihaila, A. and Fränti, P. 2005. Eye-Movements as a Biometric. Image Analysis, 780-789.

Breiman, L. 2001. Random Forests. *Machine Learning* 45, 1, 5-32.

Cortes, C. and Vapnik, V. 1995. Support-Vector Networks. *Machine Learning* 20, 273-297.

Crihalmeanu, S. and Ross, A. A. 2012. Multispectral Scleral Patterns for Ocular Biometric Recognition. *Pattern Recognition Letters* 33, 1860-1869.

Daugman, J. 2004. How Iris Recognition Works. *IEEE Transactions on Circuits and Systems for Video Technology* 14, 1, 21-30.

Duchowski, A. T. 2007. Eye Tracking Methodology: Theory and Practice. 1-360.

Hair, J. F., Tatham, R. L., Anderson, R. E. and Black, W. 1998. Multivariate Data Analysis.

Harmon, L. D., Khan, M. K., Lasch, R. and Ramig, P. F. 1981. Machine Identification of Human Faces. *Pattern Recognition* 13, 2, 97-110.

Holland, C. D. and Komogortsev, O. V. 2011. Biometric Identification via Eye Movement Scanpaths in Reading. In *International Joint Conference on Biometrics (IJCB)*, IEEE, 1-8.

Holland, C. D. and Komogortsev, O. V. 2012. Biometric Verification via Complex Eye Movements: The Effects of Environment and Stimulus. In *Fifth Internation Conference on Biometrics: Theory, Applications and Systems (BTAS)*, IEEE, 1-8.

Hotelling, H. 1931. The Generalization of Student's Ratio. *The Annals of Mathematical Statistics* 2, 3, 360-378.

Jain, A. K., Flynn, P. and Ross, A. A. 2007. Handbook of Biometrics. 1-556.

Jain, A. K., Hong, L. and Kulkarni, Y. 1999. A Multimodal Biometric System Using Fingerprint, Face, and Speech. In *International Conference on Audio- and Video-Based Biometric Person Authentication (AVBPA)*, 182-187.

Jain, A. K., Hong, L. and Pankanti, S. 2000. Biometric Identification. *Communications of the ACM* 43, 2, 90-98.

Joachims, T. SVM-Light Support Vector Machine. Available: http://svmlight.joachims.org/

Kasprowski, P. and Ober, J. 2004. Eye Movements in Biometrics. In *European Conference on Computer Vision (ECCV)*, Springer-Verlag, 248-258.

Komarinski, P. D. 2004. Automated Fingerprint Identification Systems (AFIS). 1-312.

Komogortsev, O. V. 2012a. Eye Movement Biometric Database v1. Available: http://cs.txstate.edu/~ok11/embd_v1.html

Komogortsev, O. V. 2012b. Eye Movement Biometric Database v2. Available: http://cs.txstate.edu/~ok11/embd_v2.html

Komogortsev, O. V., Gobert, D. V., Jayarathna, U. K., Koh, D. H. and Gowda, S. M. 2010. Standardization of Automated Analyses of Oculomotor Fixation and Saccadic Behaviors. *IEEE Transactions on Biomedical Engineering* 57, 11, 2635-2645.

Komogortsev, O. V., Holland, C. D. and Jayarathna, U. K. 2012a. Two-Dimensional Homeomorphic Oculomotor Plant Mathematical Model. 1-12.

Komogortsev, O. V. and Jayarathna, U. K. S. 2008. 2D Oculomotor Plant Mathematical Model for Eye Movement Simulation. In *International Conference on BioInformatics and BioEngineering (BIBE)*, IEEE, 1-8.

Komogortsev, O. V. and Karpov, A. 2013. Liveness Detection via Oculomotor Plant Characteristics: Attack of Mechanical Replicas. In *IEEE/IAPR International Conference on Biometrics (ICB)*, IEEE, 1-8.

Komogortsev, O. V., Karpov, A., Holland, C. D. and Proença, H. 2012b. Multimodal Ocular Biometrics Approach: A Feasibility Study. In *Fifth International Conference on Biometrics: Theory, Applications and Systems (BTAS)*, IEEE, 1-8.

Komogortsev, O. V., Karpov, A., Price, L. R. and Aragon, C. R. 2012c. Biometric Authentication via Oculomotor Plant Characteristics. In *International Conference on Biometrics (ICB)*, IEEE/IAPR, 1-8.

Komogortsev, O. V. and Khan, J. I. 2008. Eye Movement Prediction by Kalman Filter with Integrated Linear Horizontal Oculomotor Plant Mechanical Model. In *Eye Tracking Research & Applications (ETRA) Symposium*, ACM, 229-236.

Lagarias, J. C., Reeds, J. A., Wright, M. H. and Wright, P. E. 1998. Convergence Properties of the Nelder-Mead Simplex Method in Low Dimensions. *SIAM Journal of Optimization* 9, 1, 112-147.

Leigh, R. J. and Zee, D. S. 2006. The Neurology of Eye Movements. 1-776.

Nandakumar, K., Chen, Y., Dass, S. C. and Jain, A. K. 2008. Likelihood Ratio-based Biometric Score Fusion. *IEEE Transactions on Pattern Analysis and Machine Intelligence* 30, 2, 342-347.

Noton, D. and Stark, L. W. 1971. Scanpaths in Eye Movements during Pattern Perception. *Science* 171, 3968, 308-311.

Park, U., Ross, A. A. and Jain, A. K. 2009. Periocular Biometrics in the Visible Spectrum: A Feasibility Study. In *International Conference on Biometrics: Theory, Applications, and Systems*, 1-6.

Quaia, C. and Optican, L. M. 2003. Dynamic Eye Plant Models and the Control of Eye Movements. *Strabismus* 11, 1, 17-31.

Rayner, K. 1998. Eye Movements in Reading and Information Processing: 20 Years of Research. *Psychological Bulletin* 124, 3, 372-422.

Rigas, I., Economou, G. and Fotopoulos, S. 2012. Biometric Identification Based on the Eye Movements and Graph Matching Techniques. *Pattern Recognition Letters* 33, 6, 786-792.

Salvucci, D. D. and Goldberg, J. H. 2000. Identifying Fixations and Saccades in Eye-tracking Protocols. In *Eye Tracking Research & Applications (ETRA) Symposium*, ACM, 71-78.

Schnitzer, B. S. and Kowler, E. 2005. Eye Movements during Multiple Readings of the Same Text. *Vision Research* 46, 10, 1611-1632.

Silver, D. L. and Biggs, A. J. 2006. Keystroke and Eye-Tracking Biometrics for User Identification. In *International Conference on Artificial Intelligence (ICAI)*, 344-348.

Tabachnick, B. G. and Fidell, L. S. 2006. Using Multivariate Statistics.

Vapnik, V. N. 1999. The Nature of Statistical Learning Theory.

Wilkie, D. R. 1970. Muscle.

Williams, J. M. 2002. Biometrics or… Biohazards? In *2002 Workshop on New Security Paradigms*, 97-107.

Wiskott, L., Fellous, J.-M., Krüger, N. and Malsburg, C. v. d. 1997. Face Recognition by Elastic Bunch Graph Matching. *IEEE Transactions on Pattern Analysis and Machine Intelligence* 19, 7, 775-779.